HHS Public Access

Author manuscript

*Org Biomol Chem*. Author manuscript; available in PMC 2015 July 07.

Published in final edited form as:

*Org Biomol Chem*. 2014 July 7; 12(25): 4421–4431. doi:10.1039/c3ob42379d.

# Development of a PET Radiotracer for Noninvasive Imaging of the Reactive Oxygen Species, Superoxide, *in vivo*

**Wenhua Chu**[1], **Andre Chepetan**[2], **Dong Zhou**[1], **Kooresh I. Shoghi**[1], **Jinbin Xu**[1], **Laura L. Dugan**[2], **Robert J. Gropler**[1], **Mark A. Mintun**[1], and **Robert H. Mach**[*,1]

[1]Department of Radiology, Washington University School of Medicine, St. Louis, MO 63110, USA

[2]Division of Geriatric Medicine, Departments of Medicine and Neuroscience, University of California-San Diego, La Jolla, CA 92093

## Abstract

Reactive oxygen species (ROS) have been implicated in the pathogenesis of a wide range of human disease states and drug toxicities, but development of imaging tools to study ROS biology *in vivo* remains a challenge. Here we synthesized and validated a novel PET tracer (**12**) and its $^{18}$F radiolabeled version [$^{18}$F]**12** to allow PET (positron emission tomography) imaging of superoxide in vivo. Initial analysis of ROS reaction kinetics found that compound **12** was rapidly and selectively oxidized by superoxide, but not other ROS. Cell culture studies in EMT6 cells exposed to the cancer chemotherapeutic agent Doxorubicin (DOX), which activates the superoxide-generating enzyme, NADPH oxidase, showed that compound **12** was a sensitive and specific probe for superoxide in cells. The microPET imaging of heart in mice with DOX-induced cardiac inflammation observed 2-fold greater oxidation of [$^{18}$F]**12** in the DOX-treated mice compared to controls (p=0.02), the results were confirmed by distribution studies on organs subsequently removed from the mice and HPLC analysis of [$^{18}$F] radioactivity compounds. These data indicate that compound **12** is a useful PET tracer to imaging ROS *in vivo*.

### Keywords

ethidium; dihydroethidium; reactive oxygen species; superoxide; PET imaging

Address correspondence to: Robert H. Mach, Ph.D., University of Pennsylvania, Chemistry Building, Room 283, 231 S. 34th St, Philadelphia, PA 19104, rmach@mail.med.upenn.edu.

**Author contributions**

W.C. conducted the organic synthesis and wrote the paper, A.C. conducted the *in vitro* assays measuring the reactivity of the probes, D.Z. conducted the radiolabeling reactions and *in vivo* metabolism studies, K.I.S. designed the *in vivo* imaging, metabolism studies and analyzed the microPET image data, J.X. conducted the cell culture experiments, L.L.D. supervised the in vitro evaluation of the imaging probes and edited the paper, R.J.G. M.A.M. designed the *in vivo* imaging study, and R.H.M. designed the imaging probes and edited the paper.

**Competing financial interests**

The authors declare no competing financial interests.

**Additional information**

Supplementary information and chemical compound information is available in the online version of the paper.

## Introduction

Chronic inflammatory response in multiple diseases results in the activation of innate immune enzymes such as NADPH oxidase to produce reactive oxygen species (ROS), which in turn have been shown in animal models to contribute to tissue injury, fibrosis, remodeling and organ dysfunction for a range of pathology and disease. ROS are produced by normal cellular metabolism, and are fundamental to cell biology in a broad sense. However, while ROS are involved in all aspects of normal cellular function, disruption of the physiological balance in ROS homeostasis caused by disease, injury, or environmental stress (e.g., ionizing radiation, UV and heat exposure) can lead to inappropriate cell signaling, dysfunction, and overt cell death. At the organ level, these pathological responses to ROS can produce inflammation, fibrosis, tissue remodeling, and trigger other deleterious cascades in diseases processes such as ischemia and reperfusion of heart, lung, brain and kidney[1–5], neurodegenerative diseases including Parkinson's disease, Amyotrophic Later Sclerosis (ALS) and Alzheimer's disease[6–9], as well as end-organ fibrosis and failure in diabetes[10]. Collectively, ROS comprise the chemically reactive products of molecular oxygen ($O_2$) including the one-electron reduction product of molecular oxygen: superoxide ($O_2^{-}$)[11]. Superoxide can be produced by a number of sources *in vivo*, including the mitochondrial electron transport chain and NADPH oxidase(s), which are activated under conditions of inflammation, ischemia, and tissue injury. Superoxide has been shown to regulate distinct signaling cascades and to have specific molecular targets. The ability to detect elevated ROS in the intact animal or patient would provide a better understanding of the links between ROS, tissue injury, and disease. Furthermore, the ability to selectively identify the ROS being generated will be critical to understanding the molecular cascades affected.

A variety of methods for evaluating ROS in cell culture and tissue slices have been developed, and these approaches have advanced our understanding of both the physiological role of ROS as signaling molecules and necessary intermediates in cell metabolism, and as toxic species which can damage cells and tissues. Techniques currently employed include chemiluminescence assays[12,13], electron spin resonance (ESR) using nitrone or nitroxide spin traps[14], and fluorescence-based techniques with oxidizable fluorescent probes such as Peroxy Green 1, Peroxy Crimson 1[15,16], 2,7-dichlorodihydrogluorescein diacetate (DCFH-DA)[17–20], dihydrorhodamine 123 (DHR)[21], hydrocyanines[22,23] (see Supporting Information, Figure S1), and dihydroethidium (DHE, Figure 1) and its analogs[24–30]. Although there is an unmet need for imaging tools to study the production of metabolic and inflammatory ROS and/or reactive nitrogen species (RNS) in humans or animal models, some considerable difficulties must be overcome to develop such tools. First, ROS (and RNS) are small molecules which have a relatively short lifetime, so it cannot be detected by conventional "radioligand bound to target" strategies. Second, fluorescence, chemiluminescence, optical, and electron spin resonance imaging are limited in their ability to measure *in vivo* intracellular ROS due to substantial attenuation of the output signal by the tissue within a few centimeters. Given the drawbacks in the use of these probes, especially for imaging *in vivo* ROS production in an intact animal or human, an alternative,

sensitive method for detecting superoxide produced in a variety of biological systems is needed.

Positron emission tomography (PET) is a noninvasive imaging technique capable of measuring specific chemical or enzymatic reactions in tissues *in vivo*. Therefore, a radiolabeled DHE analog as a PET tracer to image ROS *in vivo* could overcome the disadvantages of existing DHE-based fluorescence probes. Like DHE, a DHE analog used as a PET radiotracer will not bind to DNA because it is a neutral molecule and its phenanthridine moiety has a nonplanar geometry. However, the oxidation products of the DHE analog by ROS, ethidium or 2-OH ethidium analogs, can bind to DNA since these products possess a positive charge and the corresponding phenanthridine ring system has a planar geometry. Once these positively-charged oxidized analogs bind to DNA in cells, they become trapped and are retained within the cell for a longer duration while the parent DHE analog washes out of the cell rapidly. This difference in retention provides a method to quantify ROS levels *in vivo* by PET imaging. To date, there have been no reported noninvasive or minimally invasive methods to evaluate ROS in the intact organism using PET. Here, we report the novel development of a PET-based DHE analog which could be used as a radiotracer for imaging superoxide levels in vivo.

## Results and discussion

### Synthesis of 10 and 12

The synthesis of standard compound **12** and the precursor compound **10** are shown in Scheme 1 and Scheme 2. The 4,4'-dinitrobiphenyl-2-amine (**1**) and 4-methoxybenzoyl chloride were heated in chlorobenzene to give compound **2**. The nitro groups of **2** were reduced to amines with ammonium formate using $Pd(OH)_2$ as a catalyst to afford **3**. The amine groups of **3** were protected with methyl carbamate, then cyclized with $POCl_3$ to give **4** and **5**, respectively. Compound **5** was deprotected with 48% HBr under reflux to afford the intermediate **6**. The amine groups of **6** were protected with t-butyl carbamate, and the OH group of the phenol was propynylated with 3-bromoprop-1-yne using $K_2CO_3$ as a base to give **7** and **8**, respectively. Compound **8** was methylated with $CH_3I$ in THF to afford **9**, which was reduced with $NaBH_3CN$ to give the precursor compound **10**. Compound **10** underwent copper (I)-assisted 1,3-dipolar cycloaddition with 2-fluoroethyl azide (i.e., the “Click reaction”) to yield **11**, then the Boc group was deprotected to provide the DHE analog **12**. Compound **14**, the oxidized form of **12**, was similarly synthesized from the intermediate **9** by Click reaction to afford **13**, followed by deprotection of the Boc groups to give **14**.

### Selectivity studies

After compound **12** was synthesized, its selective reactivity with different reactive oxygen species was investigated and compared to results obtained with DHE in a fluorescence plate reader assay. Compound **12** was oxidized by superoxide generated through either xanthine oxidase metabolism of hypoxanthine or by thermal decomposition of SIN-1 in the presence of CPTIO. In the both test systems, oxidation of compound **12** was completely prevented by the addition of superoxide dismutase (SOD) (Figure 2). Compound **12** was also exposed to

$H_2O_2$ alone or in the presence of horseradish peroxidase (HRP) to generate hydroxyl free radical. The fluorescence intensity results indicate that compound **12** has little reactivity with hydroxyl radical (Figure 2), or $H_2O_2$. These data suggest that **12** has good selectivity for superoxide.

## Cell studies

As with DHE, compound **12** has no fluorescence at 595 nm, but its oxidized form **14** has very strong fluorescence at 595 nm (data not shown). Therefore, fluorescence at 595 nm can be used as an indicator of the oxidation of **12**. In order to help guide PET imaging studies, we explored the ability of **12** to detect ROS induced by the anticancer drug Doxorubicin (DOX) using cancer cells growing under cell culture conditions as a model system. Mouse mammary adenocarcinoma (EMT6) cells were first treated with 400 nM DOX, after 5 h, EMT6 cells were then incubated with 2 μM DHE or 2 μM **12** for 60 min at 37 °C in the dark. Upon removal of the culture media, fluorescence intensities of the cells were measured using absorption/emission wavelengths of 480/595 nm, respectively. These results (Figure 3) showed that the fluorescence intensity significantly increased in EMT6 cells treated with DOX for both DHE and **12** in comparison with non-treated EMT6 cells. The nuclear localization of the fluorescence in the DOX-treated cells confirms that oxidation of **12** leads to trapping of the probe by intercalation into DNA. These data indicate that **12** can measure DOX-induced superoxide production in intact cancer cells.

## Radiolabeling of 12

The radiotracer [$^{18}$F]**12** was synthesized using copper (I) catalyzed Click reaction with [$^{18}$F]**16** (Scheme 3). [$^{18}$F]**16** was efficiently synthesized by an improved vacuum distillation method[31]. The Boc groups of precursor **10** were first removed with TFA to afford **17**, then [$^{18}$F]**16** was distilled into the solution of **17** in DMF, followed by the addition of a mixture of copper sulfate and sodium ascorbate as the Cu(I) source. [$^{18}$F]**12** was obtained with a yield of 42.8% (non-decay corrected) after reversed phase HPLC purification and solid phase extraction. Ascorbic acid was added to the final dose to stabilize [$^{18}$F]**12** from autoxidation. (For analytical HPLC conditions see Supporting Information, Figure S3 and S4). The total synthesis time was 120 min. The final dose in 10% ethanol/saline had a specific activity of 1.3-2.4×$10^{10}$ Bq/μmol with a radiochemical purity of 90–100%. [$^{18}$F]**14**, the oxidized form of [$^{18}$F]**12**, was generated by oxidation of [$^{18}$F]**12** with $CuSO_4$ in DMSO.

## Cell uptake studies of [$^{18}$F]12

In order to be used as a PET radiotracer for imaging intracellular superoxide, the uncharged DHE analog **12** should cross membranes get in and out cell easily, but the oxidation products of **12** by ROS, **14**, should not cross the cell membrane and should have a low cell uptake. Furthermore, once inside the cell, the compound **12** does not bind to DNA in the nucleus because it is both uncharged and nonplanar, whereas oxidation of **12** to **14** leads to a charged, planar compound which can intercalate into DNA. Once **14** binds to DNA in cells, it becomes trapped intracellularly and is retained for a longer time while the parent **12** washes out of the cell rapidly. This difference in retention provides a method to quantify ROS levels *in vivo* by PET imaging. Although it is not possible to measure the rate of

washout of **12** and **14** from cells, it is possible to measure the ability of **12** and **14** cross the membrane and enter the cell by using [$^{18}$F]**12** and [$^{18}$F]**14**. Therefore, studies of the uptake kinetics of [$^{18}$F]**12** and its oxidized form, [$^{18}$F]**14**, were carried out using EMT6 cells. Wild-type EMT-6 cells have minimal expression of p-glycoprotein[32]; therefore, active transport of [$^{18}$F]**12** and [$^{18}$F]**14** from tumor cells is not expected to occur. In this experiment, the non-charged DHE analog, **12**, should be cell-permeable and enter the cell easily, while its oxidized state, **14**, which has a positive charge, should be not cross the cell membrane. Therefore, radiolabeling of [$^{18}$F]**12** and [$^{18}$F]**14** allowed us to easily measure the kinetics of cellular uptake in both the uncharged (**12**) and charged (**14**) forms of the molecule. A $5.6\times10^6$ Bq/ml aliquot of either [$^{18}$F]**12** or [$^{18}$F]**14** was incubated with EMT6 cells for 30 min at 37 °C, then the radioactivity within the cells was counted. The results are shown in Figure 4. As expected, uptake in EMT6 cells of the oxidized form, [$^{18}$F]**14**, was much lower than uptake of the uncharged form, [$^{18}$F]**12**, indicating that the neutral species rapidly enters the cell whereas the oxidized form [$^{18}$F]**14** does not cross the cell membrane easily because of its permanent positive charge.

## MicroPET, biodistribution and stability studies of [$^{18}$F]12

A mouse model of DOX-induced cardiotoxicity was used for the in vivo evaluation of [$^{18}$F]**12**. It is currently believed that chemotherapy-induced cardiotoxicity of DOX is caused via the generation of superoxide and other ROS in cardiac tissue[33–35]. DOX-treated mice and salinetreated controls were injected with [$^{18}$F]**12** for dynamic microPET imaging studies. Initial uptake of the radioactive counts in heart was similar between treated and untreated mice. However, 1 h later, the radioactive uptake was on average ~2 fold higher in the DOX-treated mice in heart than that in the control hearts (n=4) (Figure 5). Post-microPET biodistribution data were obtained to further confirm the microPET results (see Supporting Information, Figure S5), and these data were in good agreement with the microPET data in that the radioactive uptake in the heart of DOX-treated mice was higher than that of control mice.

To further verify the result of the kinetics and stablity of [$^{18}$F]**12** in vivo and in vitro, blood and heart samples from control mice were incubated *in vitro* for 5 and 60 min. Results of HPLC anaysis showed that [$^{18}$F]**12** is stable in saline-treated control mice, where only a minimal amount of the oxidized form of [$^{18}$F]**12**, [$^{18}$F]**14** was observed at 60 min. (see Supporting Information, Figure S6). After 60 min injection of [$^{18}$F]**12** in DOX treated mice, HPLC analysis demonstrated that the blood samples contained very low levels of [$^{18}$F]**14**. However, little or no [$^{18}$F]**12** was present in the heart and only the oxidized form of [$^{18}$F]**12**, [$^{18}$F]**14**, was detected. These results show that [$^{18}$F]**12** was stable in the blood of DOX-treated mice and was oxidized to [$^{18}$F]**14** by of DOX-induced generation of ROS in the hearts of treated mice (see Supporting Information, Figure S6). HPLC analysis results confirmed that the 60 min uptake in the heart of DOX-treated mice measured by microPET and biodistribution comes from [$^{18}$F]**14**, the oxidized form of [$^{18}$F]**12**. To assess the contribution of the oxidized compound, [$^{18}$F]**14** was injected into saline-treated and DOX-treated mice. As observed in Figure 5, there were no differences in the kinetics of [$^{18}$F]**14** in saline and DOX treated mice. In both saline and DOX treated mice, [$^{18}$F]**14** clears cardiac tissue within 2sec and reaches steady-state above background levels, but well below SUV

levels of [$^{18}$F]**12** (Figure 5). The background uptake may be attributed to non-specific uptake and binding of [$^{18}$F]**14** to DNA, proteins and other moieties due to its electrostatic charge.

## Discussion

It is currently believed that elevated levels of ROS such as superoxide play a contributing role in a wide variety of pathological conditions. However, much of the evidence supporting this hypothesis has been generated in cellular or animal models of disease using fluorescent, chemiluminescent, and optical imaging techniques to measure ROS levels. Although valuable information has been gained in these preclinical studies, there is a need to develop a strategy for measuring ROS levels which could be used in translational imaging studies in humans. The goal of the current study was to develop a radiotracer which could be used to study disease-associated increases in ROS with the molecular imaging technique, PET. For this study, we synthesized a $^{18}$F-labeled analog of DHE (i.e., [$^{18}$F]**12**) a well-characterized fluorescent probe for measuring superoxide levels in vitro and in vivo, and conducted a series of studies aimed at characterizing its ability to measure ROS in vivo with PET. The results of our in vitro studies suggest that compound **12** behaves in a manner very similar to DHE. That is, the parent, neutral compound crosses the cell membrane and is oxidized by ROS (i.e., superoxide) to form a planar, permanently charged species which is retained in the cell by intercalation into DNA.

DOX is a highly effective anticancer drug that is frequently employed to treat hematological and solid tumors including leukemia, breast cancer, and soft tissue sarcomas. However, the therapeutic effectiveness of DOX is compromised by its dose dependent and cumulative cardiotoxic side effects which include cardiomyopathy. The mechanisms responsible for DOX-induced cardiomyopathy remain unclear, but it is widely accepted that the DOX-induced cardiotoxicity is mainly attributed to the initial formation of superoxide and other ROS[33–35]. It has previously been reported that DOX induces NADPH oxidase-2 (Nox2, the respiratory burst oxidase) in heart muscle. Therefore, DOX-induced ROS production in the mouse heart provided a valuable model for the *in vivo* evaluation of [$^{18}$F]**12**. In the microPET imaging study, [$^{18}$F]**12**, like DHE, does not bind to DNA because it is a neutral molecule and its phenanthridine moiety has a nonplanar geometry, thus it easily gets in and out of cells in uptake studies. In contrast, [$^{18}$F]**14**, the oxidized form of [$^{18}$F]**12**, should be trapped inside cells because it can bind to DNA due to its permanent positive charge and its planar geometry. Once positively-charged [$^{18}$F]**14** is bound to DNA, it is trapped intracellularly and retained for a longer time whereas the parent compound, [$^{18}$F]**12**, washes out of the cell quickly. Since [$^{18}$F]**14** is formed by the ROS-based oxidation of [$^{18}$F]**12**, the difference in retention of radioactivity between two tissues or two conditions (i.e., control versus patient group) should provide an effective method to quantify differences in ROS levels *in vivo* with PET imaging.

Our MicroPET imaging results show that the initial uptake of radioactivity in heart was similar between DOX-treated and untreated mice, suggesting that the DOX treatment does not alter tissue penetration of the uncharged [$^{18}$F]**12**. However, at 60 min, the radioactive uptake is ~2 fold higher in the DOX-treated mice heart than that in the control hearts (n=4).

These imaging results can be explained by the ROS induced by DOX in the hearts of DOX-treated mice. The initial cardiac uptake represents [$^{18}$F]**12** which is delivered to the hearts of both treated and untreated mice. After 60 min, most of the [$^{18}$F]**12** has washed out in the hearts of untreated mice where there is minimal ROS production, but the [$^{18}$F] signal remains elevated in the hearts of DOX-treated mice, consistent with intracellular oxidation of [$^{18}$F]**12** to [$^{18}$F]**14** by ROS, which due to its positive charge, then binds to DNA and is retained in the heart for an extended duration. Indeed, *w*hen the oxidized form of [$^{18}$F]**12**, [$^{18}$F]**14**, was injected to saline and DOX treated mice, there were no differences in the kinetics of [$^{18}$F]**14** between the groups, suggesting that retention of [$^{18}$F]**12** is specific to the reaction with superoxide to produce [$^{18}$F]**14**, in particular in DOX-treated mice where one would expect higher ROS levels. Therefore, the activity retained in the hearts at 60 min in the DOX-treated mice represents [$^{18}$F]**14**. Similarly, consistent with the microPET imaging results, the time-activity curve (TAC) showed that there was a significantly higher SUV in the myocardium of DOX-treated mice compared to hearts from untreated mice. The difference between treated and untreated mice at 60 min reflects the increased level of the ROS in the heart of DOX-treated mice. Finally, the low fluorescence of the untreated EMT cells and high accumulation of fluorescent signal in the nucleus of DOX-treated cells is consistent with our proposed mechanism of trapping of [$^{18}$F]**12** in the hearts of DOX-treated mice. This study is also a good example of the advantage of having a duo-function, optical/PET probe in characterizing the mechanism of accumulation of a PET radiotracer in tissue.

The 60 min biodistribution data indicate the DOX-treated mice have a two-fold higher retention in heart tissue compared to untreated mice, which is consistent with the results of the microPET study. In order to further confirm that the radioactive species in the hearts of DOX-treated mice at 60 min is [$^{18}$F]**14**, the in vitro stability of [$^{18}$F]**12** was evaluated by HPLC in blood and heart at 5 and 60 min. HPLC analysis showed that [$^{18}$F]**12** is stable in blood and hearts of untreated mice for 60 min. In contrast, the HPLC analysis in vivo at 60 min showed that the parent compound, [$^{18}$F]**12**, was the main component in blood and it had been completely oxdized to [$^{18}$F]**14** in heart in DOX-treated mice. This is consistent with the hypothesis that the initial cardiac uptake in the microPET imaging studies in both the DOX-treated and untreated mice is from [$^{18}$F]**12**, and the prolonged retention and higher SUVs in the DOX-treated animals is caused by the higher levels of ROS (and subsequent formation of [$^{18}$F]**14**) in the drug-treated group. The biodistribution data and the HPLC analysis results confirmed that the presence of the oxidized form of [$^{18}$F]**12**, [$^{18}$F]**14**, in heart tissue of DOX-treated mice. All of the data suggest that [$^{18}$F]**12** is capable of imaging ROS levels in intact cells and tissues using the *in vivo* imaging technique, PET.

In conclusion, abnormal production or inadequate elimination of ROS has been linked to a broad array of disease conditions, including Alzheimer's disease, diabetes, heart failure, cancer, neurodegeneration and the aging process itself. The pharmaceutical industry has actively pursued therapeutic attempts to diminish oxidative stress produced by ROS in patients and in animal models of disease. There is a growing consensus that there is a need to develop tools which will allow researchers to better understand the temporal, spatial, and biochemical contributions of ROS to normal biology as well as disease pathology. To date,

techniques to carry out such studies in humans using non-invasive imaging techniques do not exist. Thus, there is a pressing need to develop new imaging approaches which can allow clinical measurement of ROS. The current study demonstrates the development of a novel PET tracer to image and dynamically monitor biological ROS. Our data suggest that compound **12** is a useful and sensitive probe to detect superoxide *in vitro* and *in vivo*. Furthermore, the radiolabeled molecule [$^{18}$F]**12** is a promising PET tracer for the noninvasive imaging of ROS *in vivo* with PET.

## Experimental Section

### General methods and materials

All chemicals were obtained from standard commercial sources and used without further purification. All reactions were carried out using standard air-free and moisture-free techniques under an inert nitrogen atmosphere with dry solvents unless otherwise stated. Flash column chromatography was conducted using Scientific Adsorbents, Inc. silica gel, 60A, "40 Micron Flash" (32–63 μm). Melting points were determined by using MEL-TEMP 3.0 apparatus and are uncorrected. Routine $^{1}$H and $^{13}$C NMR spectra were recorded at 300 MHz on a Varian Mercury-VX and 400 MHz on Agilent Technologies spectrometers. All chemical shifts are reported as a part per million (ppm) downfield from tetramethylsilane (TMS). All coupling constants (*J*) are given in Hertz (Hz). Splitting patterns are typically described as follows: s, singlet; d, doublet; t, triplet; m, multiple. ESI/MS was performed on a Waters ZQ 4000 single quadrupole mass spectrometer equipped with an electrospray ionization (ESI) LC-MS interface. Elemental analysis (C, H, N) was determined by Atlantic Microlab, Inc., Norcross, GA. High performance liquid chromatography (HPLC) was performed with an ultraviolet detector operating at 251 nm and a well-scintillation NaI (Tl) detector and associated electronics for radioactivity detection. An Alltech Econosil C18 250 × 10 mm semi-preparative column and Altech Altima C18 250 × 4.6 mm analytical column were used for preparation and analysis respectively.

***N*-(4,4'-Dinitrobiphenyl-2-yl)-4-methoxybenzamide (2)—**A solution of 4,4'-dinitrophenyl-2-amine **1** (10.37 g, 40 mmol) and 4-methoxybenzyl chloride (8.53 g, 50 mmol) in toluene (200 mL) was heated to reflux for 24 h, then cooled to 23 °C. The solid was filtered out, washed with ether, and recrystallized from methanol to afford 12.7 g (81%) of **2** as a white solid, mp 210.2–211.6 °C. $^{1}$H NMR (300 MHz, DMSO-$d_6$) δ 10.21 (s, 1H), 8.45 (d, *J* = 2.4 Hz, 1H), 8.27 (d, *J* = 8.4 Hz, 2H), 8.20 (dd, *J* = 8.4 Hz, 2.1 Hz, 1H), 7.80–7.71 (m, 5H), 7.01 (d, *J* = 9.0 Hz, 2H), 3.81 (s, 3H). $^{13}$C NMR (75 MHz, DMSO-$d_6$) δ 165.1, 162.2, 147.4, 147.0, 144.6, 141.4, 136.6, 131.6, 129.8, 129.6, 125.8, 123.6, 121.9, 120.8, 113.7, 55.4. Analysis (calcd., found for $C_{20}H_{15}N_3O_6$): C, (61.07, 61.11), H (3.84, 3.76), N (10.68, 10.53).

***N*-(4,4'-Diaminobiphenyl-2-yl)-4-methoxybenzamide (3)—**A mixture of **2** (3.93 g, 10.0 mmol), ammonium formate (6.31 g, 100 mmol), and 20% $Pd(OH)_2$/C (200 mg) in methanol (50 mL) and ethyl acetate (50 mL) was heated to reflux for 3 h. The catalyst was filtered out through celite, and the filtrate was evaporated under reduced pressure. The crude product was dissolved in ethyl acetate (100 mL), washed with saturated $NaHCO_3$ (50 mL),

water (50 mL), NaCl (50 mL), and dried over $Na_2SO_4$. After evaporation of the ethyl acetate under reduced pressure, the crude product was purified by flash chromatography with hexane-EtOAc (1:3) to afford 3.03 g (91%) of **3** as white solid, m.p. 161.4–162.6 °C. $^1$H NMR (300 MHz, $CDCl_3$) δ 8.05 (s, 1H), 7.99 (d, *J* = 2.1 Hz, 1H), 7.60 (d, *J* = 9.0 Hz, 2H), 7.17 (d, *J* = 8.7 Hz, 2H), 7.02 (d, *J* = 8.4 Hz, 1H), 6.87 (d, *J* = 8.7 Hz, 2H), 6.77 (d, *J* = 8.7 Hz, 2H), 6.48 (dd, *J* = 8.0 Hz, 2.1 Hz, 1H), 3.81 (s, 3H), 3.79 (s, 4H). $^{13}$C NMR (75 MHz, $CDCl_3$) δ 164.4, 162.2, 146.2, 145.8, 135.9, 130.7, 130.5, 128.6, 128.0, 127.2, 122.5, 115.5, 113.9, 110.6, 106.9, 55.3. Analysis (calcd., found for $C_{20}H_{19}N_3O_2$): C, (72.05, 71.94), H (5.74, 5.68), N (12.60, 12.53).

**Dimethyl 2-(4-methoxybenzamido)biphenyl-4,4'-diyldicarbamate (4)—**A mixture of **3** (2.67 g, 8 mmol), methyl chloroformate (1.66 g, 17.6 mmol) and triethylamine (2.02 g, 20 mmol) in $CH_2Cl_2$ (75 mL) was stirred overnight at 23 °C. The mixture was washed with water (50 mL), NaCl (50 mL) and dried over $Na_2SO_4$. After evaporation of the $CH_2Cl_2$ under reduced pressure, the crude product was purified by flash chromatography with hexane-EtOAc (1:2) to afford 3.31 g (92%) of **4** as white solid, m.p. 130.7–132.0 °C. $^1$H NMR (300 MHz, DMSO-$d_6$) δ 9.77 (s, 1H), 9.64 (s, 1H), 9.63 (s, 1H), 7.79 (d, *J* = 8.7 Hz, 2H), 7.59 (d, *J* = 1.8 Hz, 1H), 7.48-7.41 (m, 3H), 7.32 (d, *J* = 8.7 Hz, 2H), 7.30 (d, *J* = 8.7 Hz, 1H), 6.99 (d, *J* = 9.0 Hz, 2H), 3.81 (s, 3H), 3.68 (s, 3H), 3.65 (s, 3H). $^{13}$C NMR (75 MHz, DMSO-$d_6$) δ 165.0, 161.8, 154.0, 138.4, 137.9, 135.2, 133.0, 131.9, 130.2, 129.3, 128.9, 126.6, 117.9, 116.4, 113.6, 55.4, 51.6, 51.5. Analysis (calcd., found for $C_{24}H_{23}N_3O_6.0.5CH_3CH_2OCH_2CH_3$): C (64.19, 63.96), H (5.80, 5.86), N (8.64, 8.47).

**Dimethyl 6-(4-methoxyphenyl)phenanthridine-3,8-diyldicarbamate (5)—**A mixture of **4** (2.70 g, 6.0 mmol) and $POCl_3$ (25 mL) was heated to reflux for 6 h. The mixture was cooled to 23 °C, then poured into ice (200 g), neutralized with $Na_2CO_3$ to pH=8, and extracted with ethyl acetate (75 ml x 2); the combined ethyl acetate was washed with water (50 mL), saturated NaCl (50 mL), and dried over $Na_2SO_4$. After evaporation of the ethyl acetate under reduced pressure, the crude product was purified by flash chromatography with hexane-EtOAc to afford 1.97 g (76%) of **5** as yellow solid, m.p. 207.9–208.7 °C. $^1$H NMR (300 MHz, DMSO-$d_6$) δ 9.96 (s, 1H), 9.93 (s, 1H), 8.62 (d. *J* = 9.0 Hz, 1H), 8.52 (d, *J* = 9.3 Hz, 1H), 8.28 (s, 1H), 8.12 (s, 1H), 7.87 (d, *J* = 8.7 Hz, 1H), 7.69 (d, *J* = 8.7 Hz, 1H), 7.59 (d, *J* = 8.1 Hz, 2H), 7.05 (d, *J* = 8.4 Hz, 2H), 3.79 (s, 3H), 3.65 (s, 3H), 3.59 (s, 3H). $^{13}$C NMR (75 MHz, DMSO-$d_6$) δ 160.6, 160.3, 154.7, 144.0, 139.8, 138.4, 132.5, 131.7, 128.9, 125.1, 123.8, 123.3, 119.3, 119.0, 117.0, 115.8, 114.2, 55.9, 52.5, 52.4. Analysis (calcd., found for $C_{24}H_{21}N_3O_5$): C (66.81, 66.78), H (4.91, 4.80), N (9.74, 9.63).

**4-(3,8-Diaminophenanthridin-6-yl)phenol (6)—**A solution of **5** (1.73 g, 4 mmol) in 48% HBr (100 mL) was heated under reflux for 3 days, then neutralized with $Na_2CO_3$ to pH=8, and extracted with $CH_2Cl_2$ (50 mL x 2); the combined $CH_2Cl_2$ was washed with water (50 mL), NaCl (50 mL) and dried over $Na_2SO_4$. After evaporation of the $CH_2Cl_2$ under reduced pressure, the crude product was purified by flash chromatography with ethyl acetate to afford 1.10 g (91%) of **6** as brown solid, m.p. 201.4–202.3 °C. $^1$H NMR (300 MHz, DMSO-$d_6$) δ 9.69 (s, 1H), 8.30 (d, *J* = 8.7 Hz, 1H), 8.21 (d, *J* = 9.0 Hz, 1H), 7.46 (d, *J*

= 8.1 Hz, 2H), 7.15 (d, *J* = 8.7 Hz, 1H), 7.08 (s, 1H), 7.03 (s, 1H), 6.95 (m, 3H), 5.37 (s, 2H), 5.33 (s, 2H). $^{13}$C NMR (75 MHz, DMSO-$d_6$) δ 159.6, 158.0, 148.2, 146.8, 144.2, 131.9, 131.3, 125.4, 125.3, 122.9, 122.4, 121.2, 117.4, 115.4, 110.7, 109.0. Analysis (calcd., found for $C_{19}H_{15}N_3O.0.5H_2O$): C (73.53, 73.23), H (5.20, 5.51), N (13.54, 12.34).

***tert*-Butyl 6-(4-hydroxyphenyl)phenanthridine-3,8-diyldicarbamate (7)—**A mixture of **6** (1.05 g, 3.5 mmol) and di-*tert*-butyl dicarbonate (1.82 g, 8.4 mmol) in *tert*-butanol (50 mL) was stirred 2 days at 23 °C. After evaporation of the solvent under reduced pressure, the crude product was purified by flash chromatography with $CH_2Cl_2$-EtOAc (3:1) to afford 1.47 (84%) of **7** as white solid, m.p. 212.7–213.3 °C. $^1$H NMR (300 MHz, DMSO-$d_6$) δ 9.80 (s, 1H), 9.73 (s, 1H), 9.71 (s, 1H), 8.68 (d, *J* = 9.3 Hz, 1H), 8.57 (d, *J* = 9.3 Hz, 1H), 8.32 (d, *J* = 1.8 Hz, 1H), 8.18 (d, *J* = 1.8 Hz, 1H), 8.01 (d, *J* = 7.5 Hz, 1H), 7.79 (dd, *J* = 9.0 Hz, 1.8 Hz, 1H), 7.58 (d, *J* = 8.4 Hz, 2H), 6.98 (d, *J* = 8.4 Hz, 2H), 1.54 (s, 9H), 1.48 (s, 9H). $^{13}$C NMR (75 MHz, DMSO-$d_6$) δ 160.7, 158.6, 153.4, 144.0, 140.1, 138.7, 131.8, 131.0, 128.8, 125.0, 123.5, 123.1, 119.2, 118.7, 116.9, 115.9, 115.6, 80.0, 28.8, 28.7. Analysis (calcd., found for $C_{29}H_{31}N_3O_5.0.75H_2O$): C (67.62, 67.92), H (6.36, 6.61), N (8.16, 7.74).

***tert*-Butyl 6-(4-(prop-2-ynyloxy)phenyl)phenanthridine-3,8-diyldicarbamate (8)—**A mixture of **7** (1.25 g, 2.5 mmol), 80% propargyl bromide in toluene (744 mg, 5.0 mmol) and $K_2CO_3$ (1.04 g, 7.5 mmol) in acetone (50 mL) was heated under reflux for 8 h. After evaporation of the solvent, ethyl acetate (75 mL) was added, washed with water (50 mL x 2), NaCl (50 mL) and dried over $Na_2SO_4$. After evaporation of the solvent under reduced pressure, the crude product was purified by flash chromatography with $CH_2Cl_2$-EtOAc (10:1) to afford 1.28 g (95%) of **8** as white solid, m.p. 129.5–130.3 °C. $^1$H NMR (300 MHz, $CDCl_3$) δ 8.46 (d, *J* = 9.0 Hz, 1H), 8.37 (d, *J* = 9.0 Hz, 1H), 8.05 (d, *J* = 8.1 Hz, 1H), 7.91 (d, *J* = 8.7 Hz, 1H), 7.90 (s, 1H), 7.79 (d, *J* = 2.1 Hz, 1H), 7.64 (d, *J* = 8.7 Hz, 2H), 7.08 (d, *J* = 8.7 Hz, 2H), 6.95 (s, 1H), 6.89 (s, 1H), 4.74 (d, *J* = 2.4 Hz, 2H), 2.55 (t, *J* = 2.4 Hz, 1H), 1.55 (s, 9H), 1.50 (s, 9H). $^{13}$C NMR (75 MHz, $CDCl_3$) δ 160.5, 158.0, 152.7, 152.6, 143.8, 138.5, 136.9, 133.0, 131.0, 129.2, 125.2, 122.9, 122.4, 119.3, 119.0, 117.6, 116.5, 114.8, 80.9, 80.8, 78.5, 75.7, 55.9, 28.3, 28.2. Analysis (calcd., found for $C_{32}H_{33}N_3O_5.0.5H_2O$): C (70.06, 70.10), H (6.25, 6.10), N (7.66, 7.64).

**3,8-Bis(*tert*-butoxycarbonylamino)-5-methyl-6-(4-(prop-2-ynyloxy)phenyl)phenanthridinium iodide (9)—**A mixture of **8** (1.08 g, 2.0 mmol) and $CH_3I$ (5 mL) in THF (15 mL) was heated under reflux for 5 days. After removing of the solvent, ethyl ether (30 mL) was added, the precipitate solid was filtered out and washed with ethyl ether to afford 1.12 g (82%) of **9** as yellow solid, m.p. 209.4–210.0 °C. $^1$H NMR (300 MHz, DMSO-$d_6$) δ 10.27 (s, 1H), 9.98 (s, 1H), 9.01 (d, *J* = 8.4 Hz, 1H), 8.93 (d, *J* = 8.7 Hz, 1H), 8.71 (s, 1H), 8.40 (d, *J* = 8.7 Hz, 1H), 8.02 (d, *J* = 9.0 Hz, 1H), 7.77 (s, 1H), 7.69 (d, *J* = 8.4 Hz, 2H), 7.40 (d, *J* = 8.1 Hz, 2H), 5.01 (s, 2H), 4.16 (s, 3H), 3.71 (s, 1H), 1.55 (s, 9H), 1.44 (s, 9H). $^{13}$C NMR (75 MHz, DMSO-$d_6$) δ 163.6, 159.9, 153.3, 153.2, 142.9, 140.8, 136.0, 131.4, 130.2, 129.1, 126.0, 125.5, 124.7, 124.1, 122.0, 120.9, 118.4, 116.1, 81.2, 80.7, 79.4, 56.5, 43.9, 28.7, 28.6. Analysis (calcd., found for $C_{33}H_{36}IN_3O_5.0.5H_2O$): C (57.40, 57.47), H (5.40; 5.34), N (6.08, 5.91).

***tert*-Butyl 5-methyl-6-(4-(prop-2-ynyloxy)phenyl)-5,6-dihydrophenanthridine-3,8-diyldicarbamate (10)—**$NaBH_3CN$ (126 mg, 2.0 mmol) was added to a solution of **9** (682 mg, 1.0 mmol) in methanol (15 mL) and the mixture was stirred 3 h at 23 °C. After evaporation of the methanol under reduced pressure, ethyl acetate (75 mL) was added, washed with water (30 mL), NaCl (30 mL), and dried over $Na_2SO_4$. After removal of the solvent under reduced pressure, the crude product was purified by flash chromatography with $CH_2Cl_2$-ether (100:5) to afford 468 mg (84%) of **10** as white solid, m.p. 215.4–216.0 °C. $^1$H NMR (300 MHz, $CDCl_3$) δ 7.64 (d, *J* = 8.7 Hz, 1H), 7.57 (d, *J* = 8.1 Hz, 1H), 7.18 (s, 1H), 7.17 (d, *J* = 8.1 Hz, 1H), 7.02 (d, *J* = 9.0 Hz, 2H), 6.77-6.70 (m, 4H), 6.52 (s, 2H), 5.23 (s, 1H), 4.55 (d, *J* = 2.1 Hz, 2H), 2.83 (s, 3H), 2.46 (t, *J* = 2.1 Hz, 1H), 1.50 (s, 9H), 1.48 (s, 9H). $^{13}$C NMR (75 MHz, $CDCl_3$) δ 157.0, 152.5, 144.9, 139.1, 137.0, 135.7, 134.5, 127.9, 125.5, 123.0, 122.7, 117.9, 117.0, 116.4, 114.7, 107.5, 102.4, 80.4, 80.3, 78.6, 75.4, 67.2, 55.7, 37.0.28.3, 28.2. Analysis (calcd., found for $C_{33}H_{37}N_3O_5$): C (71.33, 71.47), H (6.71, 6.79), N (7.56, 7.50).

***tert*-Butyl 6-(4-((1-(2-fluoroethyl)-1*H*-1,2,3-triazol-4-yl)methoxy)phenyl)-5-methyl-5,6-dihydrophenanthridine-3,8-diyldicarbamate (11)—**A mixture of **10** (278 mg, 0.5 mmol), 1-azido-2-fluoroethane(1.05 mmol), sodium ascorbate (495 mg, 2.5 mmol), and $CuSO_4.5H_2O$ (62.5 mg, 0.25 mmol) in DMF (10 mL) was stirred overnight at 23 °C. The reaction mixture was diluted with ethyl acetate (75 mL), and washed with water (50 mL × 2), saturated NaCl (50 mL), and dried over $Na_2SO_4$. After evaporation of the solvent under reduced pressure, the crude product was purified by flash chromatography with $CH_2Cl_2$-EtOAc (100:5) to afford 229 mg (71%) of **11** as white solid, m.p. 124.7–125.5 °C. $^1$H NMR (300 MHz, $CDCl_3$) δ 7.64 (m, 2H), 7.57 (d, *J* = 8.1 Hz, 1H), 7.18 (s, 2H), 7.01 (d, *J* = 8.4 Hz, 2H), 6.73 (m, 4H), 6.56 (s, 2H), 5.21 (s, 1H), 5.07 (s, 2H), 4.74 (dt, *J* = 47.7 Hz, 4.2 Hz, 2H), 4.60 (dt, *J* = 27.6 Hz, 4.2 Hz, 2H), 2.82 (s, 3H), 1.50 (s, 9H), 1.48 (s, 9H). $^{13}$C NMR (75 MHz, $CDCl_3$) δ 157.6, 152.5, 144.9, 144.5, 139.1, 137.0, 135.7, 134.2, 128.0, 125.5, 123.6, 123.0, 122.6, 117.9, 117.0, 116.4, 114.6, 107.5, 102.4, 81.3 (d, *J* = 171.9 Hz), 80.4, 80.2, 67.1, 61.8, 50.4 (d, *J* = 20.5 Hz), 37.0, 28.3, 28.2. Analysis (calcd., found for $C_{35}H_{41}FN_6O_5$): C (65.20, 65.28), H (6.41, 6.56), N (13.03, 12.58).

**6-(4-((1-(2-Fluoroethyl)-1 *H*-1,2,3-triazol-4-yl)methoxy)phenyl)-5-methyl-5,6-dihydrophenanthridine-3,8-diamine (12)—**A mixture of **11** (161 mg, 0.25 mmol) in ethyl acetate (6 mL) and 37% HCl (2 mL) was stirred for 3 h. After evaporation of the solvent under reduced pressure, the product was dried in vacuum for 8 h to afford 138 mg (100%) of **12** (HCl salt) as pale yellow solid, m.p. 106.0–106.5 °C. $^1$H NMR (400 MHz, DMSO-$d_6$, HCl salt) δ 8.19 (s, 1H), 7.97 (d, *J* = 8.8 Hz, 1H), 7.88 (d, *J* = 8.4 Hz, 1H), 7.27 (dd, *J* = 8.2 Hz, 2.0 Hz, 1H), 7.08 (d, *J* = 1.6 Hz, 1H), 7.01 (d, *J* = 8.8 Hz, 2H), 6.86 (d, *J* = 8.8 Hz, 2H), 6.73 (dd, *J* = 8.4 Hz, 1.6 Hz, 1H), 6.56 (d, *J* = 1.6 Hz, 1H), 5.61 (s, 1H), 5.02 (s, 2H), 4.77 (dt, *J* = 46.8 Hz, 4.4 Hz, 2H), 4.67 (dt, *J* = 27.6 Hz, 4.0 Hz, 2H), 2.80 (s, 3H). $^{13}$C NMR (100 MHz, DMSO-$d_6$, HCl salt) δ 172.4, 158.2, 145.7, 143.2, 137.0, 133.8, 131.6, 130.0, 128.1, 125.4, 124.8, 124.4, 115.1, 112.1, 107.1, 82.3 (d, *J* = 167.3 Hz), 65.3, 64.9, 50.4 (d, *J* = 20.2 Hz), 36.8. Analysis (calcd., found for $C_{25}H_{25}FN_6O.2.5HCl.0.5H_2O$): C (55.13, 55.49), H (5.27, 5.34), N (15.43, 15.11).

**3,8-bis(tert-butoxycarbonylamino)-6-(4-((1-(2-fluoroethyl)-1H-1,2,3-triazol-4-yl)methoxy)phenyl)-5-methylphenanthridinium iodide (13)—**was prepared according to the same procedure for compound **11**, except using compound **9** (170 mg, 0.25 mmol), 1-azido-2-fluoroethane (0.5 mmol), sodium ascorbate (248 mg, 1.25 mmol), and $CuSO_4.5H_2O$ (32 mg, 0.13 mmol) in DMF (10 mL). The reaction mixture was diluted with water (75 mL), then extracted with $CH_2Cl_2$ (50 mL × 2), the extracted $CH_2Cl_2$ was combined, washed with water (50 mL), NaCl (50 mL) and dried over $Na_2SO_4$. After evaporation of the $CH_2Cl_2$, the crude product was recrystallized from ethyl acetate to afford **13** as yellow solid (105 mg, 55%), m.p. 156.0–157.9 °C. $^1$H NMR (400 MHz, DMSO-$d_6$) δ 10.23, 9.93, 8.97 (d, *J* = 9.6 Hz, 1H), 8.95 (d, *J* = 10.0 Hz, 1H), 8.68 (s, 1H), 8.38 (d, *J* = 7.2 Hz, 1H), 8.37 (s, 1H), 7.99 (d, *J* = 8.8 Hz, 1H), 7.75 (s, 1H), 7.64 (d, *J* = 8.4 Hz, 2H), 7.44 (d, *J* = 8.4 Hz, 2H), 5.32 (s, 2H), 4.84 (dt, *J* = 47.2 Hz, 4.8 Hz, 2H), 4.75 (dt, *J* = 27.6 Hz, 4.0 Hz, 2H), 4.13 (s, 3H), 1.51 (s, 9H), 1.41 (s, 9H). $^{13}$C NMR (100 MHz, DMSO-$d_6$) δ 163.5, 160.5, 153.1, 153.0, 145.5, 142.7, 140.6, 137.9, 135.8, 131.3, 130.0, 128.8, 128.4, 125.9, 125.3, 124.1, 123.9, 121.8, 120.6, 118.2, 115.8, 82.4 (d, *J* = 167.3 Hz), 81.0, 80.5, 61.9, 50.6 (d, *J* = 19.3 Hz), 43.8, 28.5, 28.4.

**3,8-diamino-6-(4-((1-(2-fluoroethyl)-1H-1,2,3-triazol-4-yl)methoxy)phenyl)-5-methylphenanthridinium chloride (14)—**was prepared according to the same procedure for compound **12**, except using compound **13** (77 mg, 0.1 mmol) in ethyl acetate (3 mL) and 37% HCl (1 mL) and stirred for 3 h. After evaporation of the solvent under reduced pressure, the product was dried in vacuum for 8 h to afford 55 mg (100%) of **14** (HCl salt) as red solid, m.p. 133.9–135.3 °C. $^1$H NMR (400 MHz, DMSO-$d_6$, HCl salt) δ 8.80 (d, J = 6.8 Hz, 1H), 8.74 (d, J = 7.2 Hz, 1H), 8.41 (s, 1H), 7.76-7.41 (m, 8H), 5.28 (s, 2H), 4.87-4.71 (m, 4H), 4.00 (s, 3H). $^{13}$C NMR (100 MHz, DMSO-$d_6$, HCl salt) δ 161.2, 160.3, 131.3, 128.6, 125.9, 124.3, 115.8, 82.4 (d, J = 167.3 Hz), 61.9, 50.6 (d, J = 17.8 Hz), 43.3.

## Radiosynthesis of [$^{18}$F]12

**Deprotection of 10—**Into a 10 mL Pyrex tube with screw cap was loaded **10** (2 mg, 3.51 μmol). The tube was flushed with argon before and after the addition of TFA (500 μL) and ascorbic acid (1 mg, 5.68 μmol) in water (100 μL), and then the tube was capped and wrapped with aluminum foil. The tube was shaken to dissolve **10**, and the reaction was allowed to proceed at ambient temperature for 15 min. TFA and water were then removed under vacuum (~ 1 torr) at ambient temperature to afford **17** as a pale yellow residue. This was done 1 h before labeling.

**Radiosynthesis of [$^{18}$F]12—**DMF (300 μL) and *N*, *N*-diisopropylethylamine (10 μL) were added to the previously prepared tube to dissolve **17**, and then the tube was cooled in a dry ice trap. [$^{18}$F]fluoroethylazide **16** (~ $1.3\times10^9$ Bq) in acetonitrile (200 μL), starting from [$^{18}$F]fluoride ($1.9\times10^9$ Bq), was distilled directly to the tube according to the literature. The tube was removed from the trap, and warmed up to ambient temperature in a water bath. Sodium ascorbate (15 mg, 76 μmol) in water (50 μL) and $CuSO_4\cdot5H_2O$ (5 mg, 20 μmol) in water (50 μL) was mixed to form a yellow slurry, which was added to the tube containing [$^{18}$F]**16** and **17**. The reaction mixture was shaken occasionally at ambient temperature over

10 min, and then a solution of 10% acetonitrile/water/0.1% TFA (4 mL) was added to the mixture. The solution was injected through a nylon filter (0.45 μm) for HPLC purification. Semi-preparative HPLC purification was carried out using an Agilent SB-C18 250 × 9.4 mm 5 μ column with 17% acetonitrile/water/0.1% TFA as the mobile phase at a flow rate of 4 mL/min and UV at 280 nm. [$^{18}$F]**12** was eluted at 14 min, and the desired HPLC fraction (~5.5×10$^{8}$ Bq) was collected in a 50 mL tube containing ascorbic acid (5 mg) in water (~ 10 mL). The collected eluent was further diluted with water to 50 mL, and passed through a C18 Sep-Pak (Waters, Classic), which had been pretreated with ethanol (10 mL) and a solution of ascorbic acid (1 mg/10 mL) in water (10 mL). The Sep-Pak was rinsed with the solution of ascorbic acid (10 mL), and then [$^{18}$F]**12** was eluted with ethanol (containing ascorbic acid, 1 mg/mL). The dose was formulated in 10% ethanol/saline (containing 0.1 mg ascorbic acid/mL). Total synthesis time was 90 min starting from [$^{18}$F]fluoride, yield 42.8% (non-decay corrected) starting from [$^{18}$F]**16**, radiochemical purity up to 99%, and the specific activity at the end of synthesis is 1.3-2.4×10$^{10}$ Bq/μmol.

## Conversion of [$^{18}$F]12 to [$^{18}$F]14

To a solution of [$^{18}$F]**12** in DMSO (300 μL) was added a solution of $CuSO_4 \cdot 5H_2O$ (1 mg) in water (10 μL). The mixture was shaken and checked by HPLC. [$^{18}$F]**12** was consumed quickly, and [$^{18}$F]**14** was formed as the major product (90%). The reaction mixture was diluted with water (10 mL) for solid phase extraction (Waters, C18 Classic). The [$^{18}$F]**14** was eluted with DMSO for cell study (4.8×10$^{6}$ Bq /100 μL DMSO).

## In-vivo imaging of Doxorubicin (DOX)-induced cardiotoxicity

**Animal Model—**All animal studies were carried out in accordance with the National Institute of Health Guide for the Care and Use of Laboratory Animals under protocols approved by the Washington University in St. Louis Animal Study Committee (IACUC). DOX has been shown to induce the formation of ROS, chief among them is the generation of the superoxide radical[32]. To that end, male C57BL/6 mice were divided into 2 groups (4 mice/group). The untreated group received 200 μL of saline intraperitoneal (i.p.) while the DOX-treated mice received a single i.p. injection of 20 mg/kg DOX-HCl salt. Five days post-treatment, 60 min dynamic PET imaging was performed as described below.

**Pre-Clinical PET Imaging—**Mice were anesthetized by inhalation of 2–2.5% isoflurane administered via an induction chamber. Dynamic PET acquisition was started after a bolus injection of [$^{18}$F]**12** (9.3–11.1×10$^{6}$ Bq/100 μL) via a tail vein catheter. PET imaging was performed on either the microPET Inveon or Focus-220. Scanners were cross-calibrated to ensure reliability of the data. Body temperature was maintained by a heat lamp. At the conclusion of imaging, the biodistribution of [$^{18}$F]**12** was determined in multiple organs. In addition, HPLC analysis was performed to determine the presence of parent and metabolites species in heart and blood. To evaluate the kinetics and cardiac uptake of the oxidized form, [$^{18}$F]**14** was similarly injected to untreated and DOX treated mice for comparison against the kinetics of [$^{18}$F]F**12**.

## Supplementary Material

Refer to Web version on PubMed Central for supplementary material.

## Acknowledgments

The authors would like to thank Fanjie Zhang for her technical assistance. This research was funded by grants AG36045 and 5R01EB12284 awarded by the National Institutes of Health, the Charles and Joanne Knight Alzheimer's Research Initiative of the Washington University Alzheimer's Disease Research Center (RHM), and 5R01AG033679 and the Larry L. Hillblom Foundation (LLD).

## References

1. Brieger K, Schiavone S, J. F, Miller Krause KH Jr. Swiss Med Wkly. 2012; 142:w13659. [PubMed: 22903797]
2. Winterbourn CC. Nat. Chem. Biol. 2008; 4(5):278–286. [PubMed: 18421291]
3. Sugamura K, Keaney FJ Jr. Free Radical Biol. Med. 2011; 51:978–992. [PubMed: 21627987]
4. Rosanna DP, Salvatore C. Curr. Pharm. Des. 2012; 18(26):3889–3900. [PubMed: 22632750]
5. Baud L, Ardaillou R. Br. Med. Bull. 1993; 49(3):621–629. [PubMed: 8221027]
6. Emerit J, Edeas M, Bricaire F. Biomed. Pharmacother. 2004; 58:39–46. [PubMed: 14739060]
7. Uttara B, Singh AV, Zamboni P, Mahajan RT. Curr. Neuropharmacol. 2009; 7:65–74. [PubMed: 19721819]
8. Multhaup G, Ruppert T, Schlicksupp A, Hesse L, Beher D, Masters CL, Beyreuther K. Biochem. Pharmacol. 1997; 54:533–539. [PubMed: 9337068]
9. Dumont M, Beal MF. Free Radical Biol. Med. 2011; 51:1014–1026. [PubMed: 21130159]
10. Paravicini TM, Touyz RM. Diabetes Care. 2008; 31(Suppl 2):s170–s180. [PubMed: 18227481]
11. Gomes A, Fernandes E, Lima JL. J. Biochem. Biophys. Methods. 2005; 65:45–80. [PubMed: 16297980]
12. Faulkner K, Fridovich I. Free Radical Biol. Med. 1993; 15:447–451. [PubMed: 8225026]
13. Daiber A, Oelze M, August M, Wendt M, Sydow K, Wieboldt H, Kleschyov AL, Munzel T. Free Radical Res. 2004; 38:259–269. [PubMed: 15129734]
14. Dikalov S, Jiang J, Mason RP. Free Radical Res. 2005; 39:825–836. [PubMed: 16036362]
15. Miller EW, Tulyathan O, Isacoff EY, Chang CJ. Nat. Chem. Biol. 2007; 3(5):263–267. [PubMed: 17401379]
16. Dickinson BC, Huynh C, Chang CJ. J. Am. Chem. Soc. 2010; 132(16):5906–5915. [PubMed: 20361787]
17. Rota C, Fann YC, Mason RP. J. Biol. Chem. 1999; 274:28161–28168. [PubMed: 10497168]
18. Rota C, Chignell CF, Mason RP. Free Radical Biol. Med. 1999; 27:873–881. [PubMed: 10515592]
19. Marchesi E, Rota C, Fann YC, Chignell CF. R. P. Mason. Free Radical Biol. Med. 1999; 26:148–161.
20. Wrona M, Wardman P. Free Radical Biol. Med. 2006; 41:657–667. [PubMed: 16863999]
21. Qin Y, Lu M, Gong X. Cell Biol. Int. 2008; 32:224–228. [PubMed: 17920943]
22. Kundu K, Knight SF, Willett N, Lee S, Taylor RW, Murthy N, Chem Angew. Int. Ed. Engl. 2009; 48:299–303.
23. Kundu K, Knight SF, Lee S, Taylor RW, Murthy N, Chem Angew. Int. Ed. Engl. 2010; 49:6134–6138.
24. Zielonka J, Zhao H, Xu Y, Kalyanaraman B. Free Radical Biol. Med. 2005; 39:853–863. [PubMed: 16140206]
25. Garbett NC, Hammond NB, Graves DE. Biophys. J. 2004; 87:3974–3981. [PubMed: 15465858]
26. Zielonka J, Vasquez-Vivar J, Kalyanaraman B. Nat. Protoc. 2008; 3(1):8–21. [PubMed: 18193017]
27. Zhao H, Kalivendi S, Zhang H, Joseph J, Nithipatikom K, Vasquez-Vivar J, Kalyanaraman B. Free Radical Biol. Med. 2003; 34:1359–1368. [PubMed: 12757846]

28. Zielonka J, Kalyanaraman B. Free Radical Biol. Med. 2010; 48:983–1001. [PubMed: 20116425]
29. Zhao H, Joseph J, Fales HM, Sokoloski EA, Levine RL, Vasquez-Vivar J, Kalyanaraman B. Proc. Natl. Acad. Sci. U. S. A. 2005; 102:5727–5732. [PubMed: 15824309]
30. Fink B, Laude K, McCann L, Doughan A, Harrison DG, Dikalov S. Am. J. Physiol.: Cell Physiol. 2004; 287:C895–C902. [PubMed: 15306539]
31. Zhou D, Chu W, Dence CS, Mach RH, Welch MJ. Nucl. Med. Biol. 2012; 39(8):1175–81. [PubMed: 22770647]
32. Patel KJ, F Tannock I. BMC Cancer. 2009; 9:356. [PubMed: 19807929]
33. Mukhopadhyay P, Rajesh M, Batkai S, Kashiwaya Y, Hasko G, Liaudet L, Szabo C, Pacher P. Am. J. Physiol.: Heart Circ. Physiol. 2009; 296:H1466–H1483. [PubMed: 19286953]
34. Shen F, Chu S, Bence AK, Bailey B, Xue X, Erickson PA, Montrose MH, Beck WT, Erickson LC. J. Pharmacol. Exp. Ther. 2008; 324(1):95–102. [PubMed: 17947497]
35. Fu Z, Guo J, Jing L, Li R, Zhang T, Peng S. Toxicol. In Vitro. 2010; 24:1584–1591. [PubMed: 20600803]

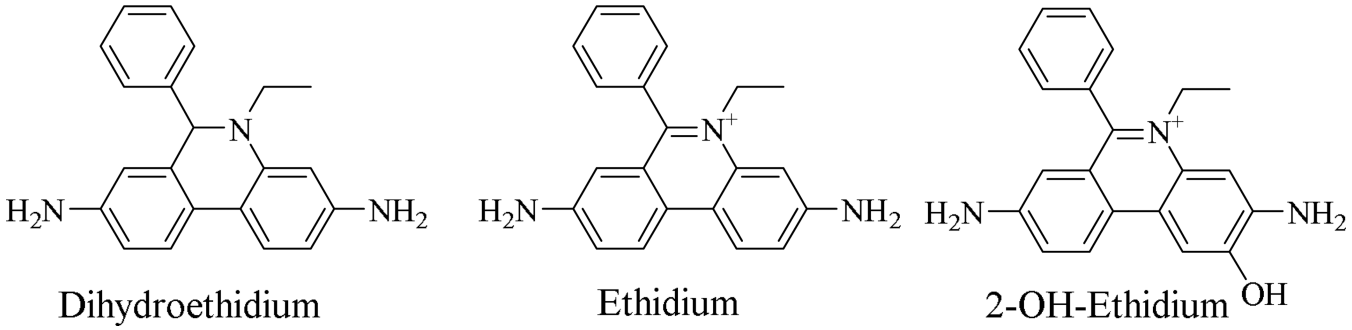


**Figure 1.**
Structures of dihydroethidium, ethidium and 2-OH-ethidium

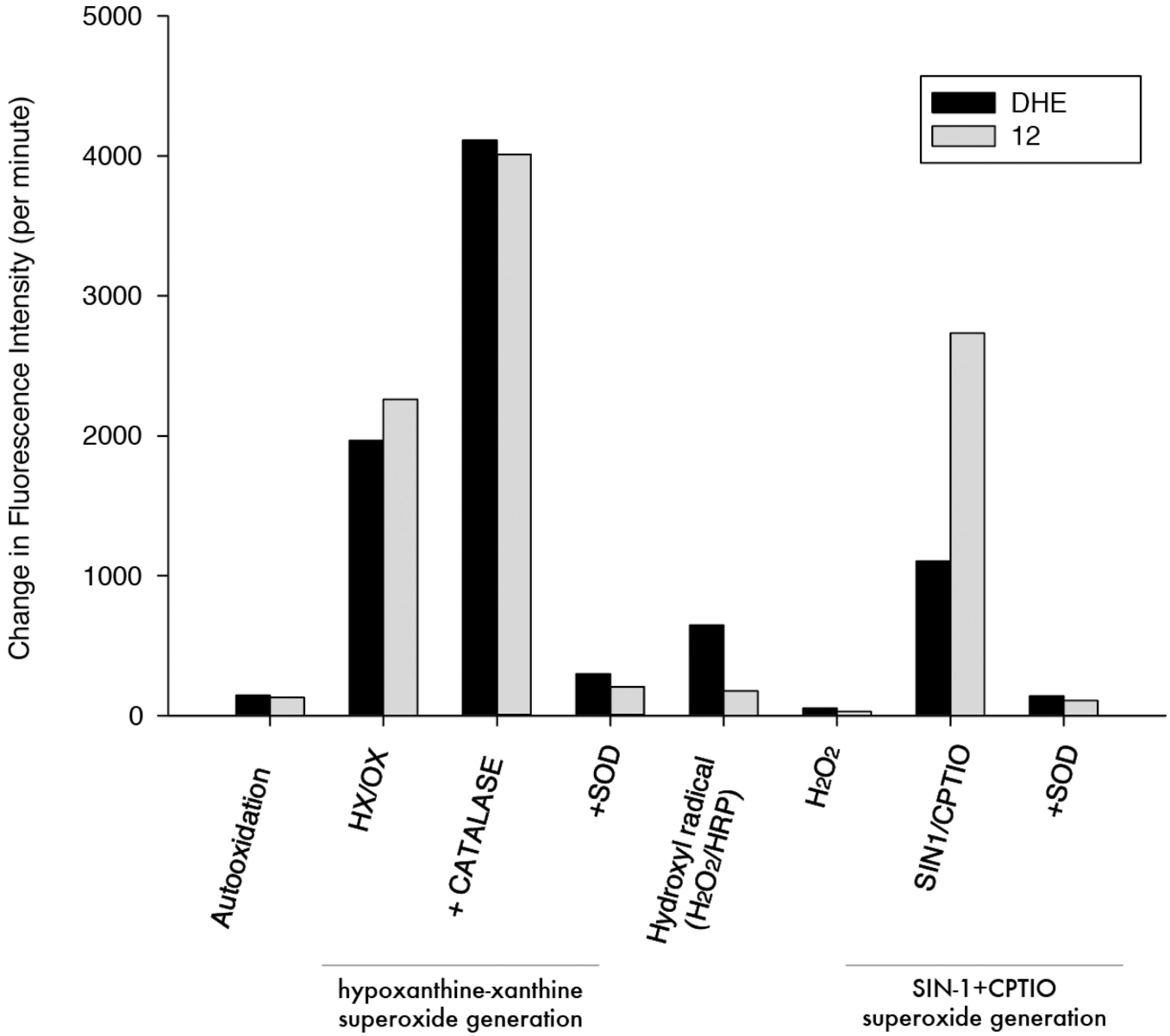


**Figure 2.**
Compounds **12** and DHE for selective reactivity with superoxide radical.

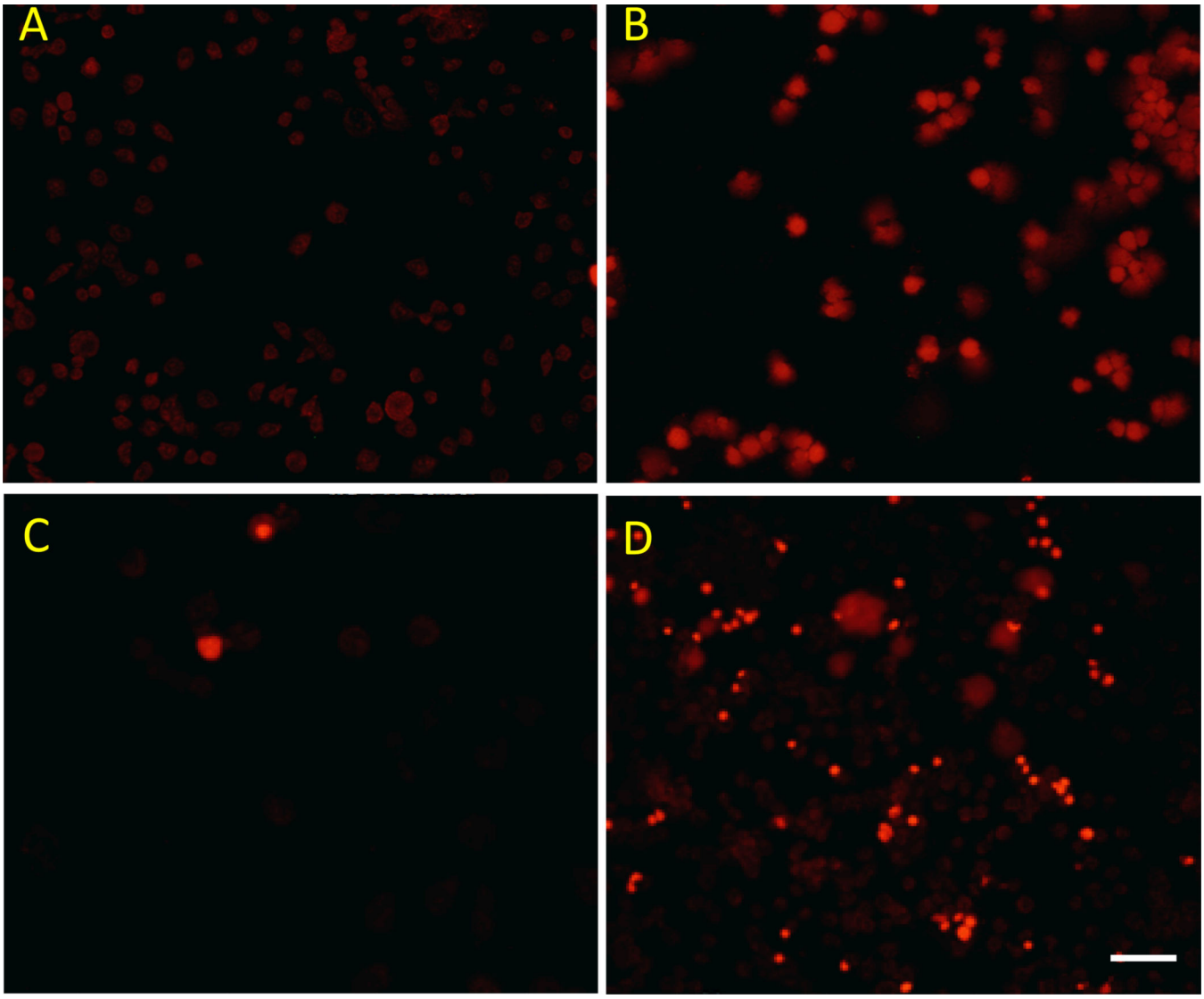


**Figure 3.**

Fluorescence imaging of ROS induced by anticancer drug doxorubicin treatment in EMT6 cells. Control cells (A and C) and doxorubicin-treated EMT6 cells (B and D) were imaged using either 2 μM DHE (A and B) or 2 μM **12** (C and D). Doxorubicin-treated cells displayed increased fluorescence signal for both compounds. Scale bar represents 100 μm.

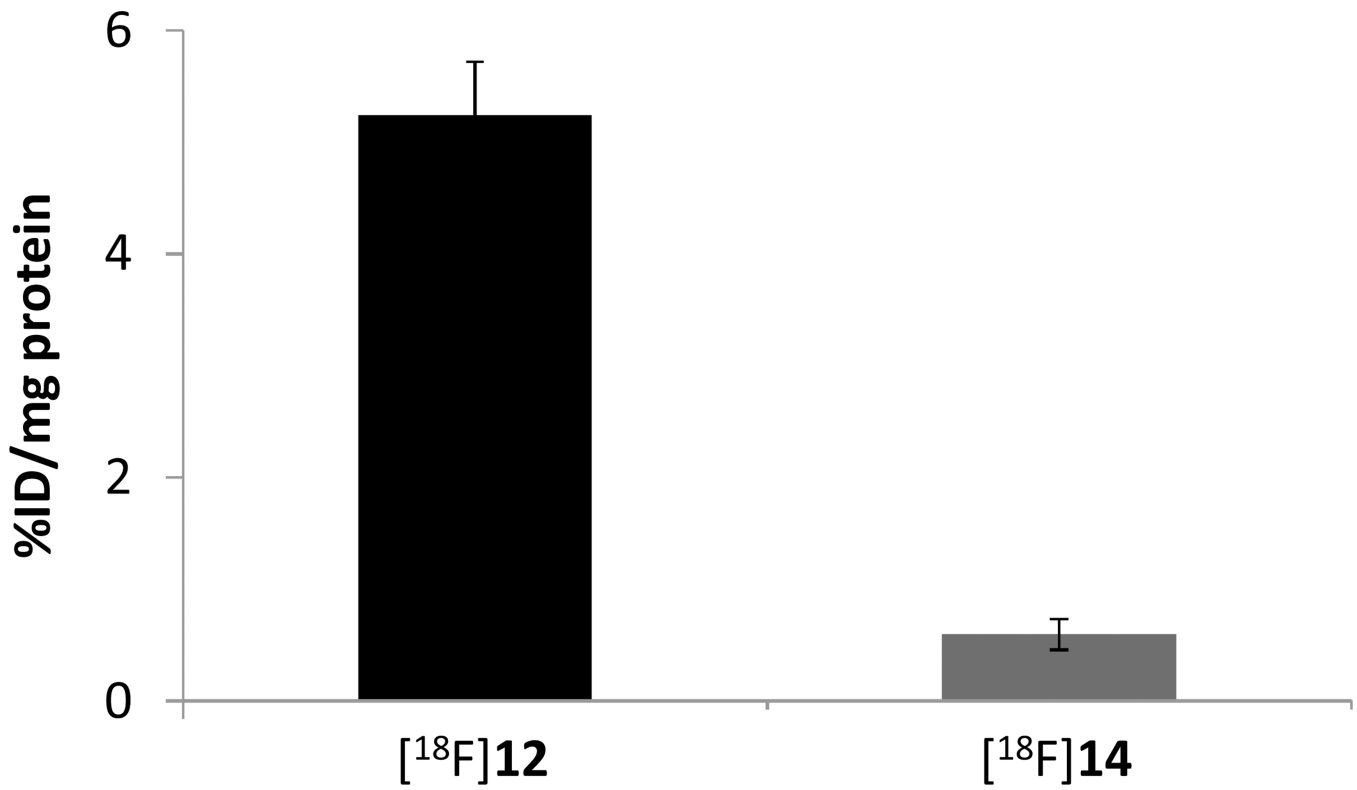


**Figure 4.**

EMT-6 cell uptake assay of [$^{18}$F]**12** and the oxidized compound [$^{18}$F]**14**. Uptake of [$^{18}$F]**12** was significantly higher than that of [$^{18}$F]**14** $p \ll 0.001$, student t test.

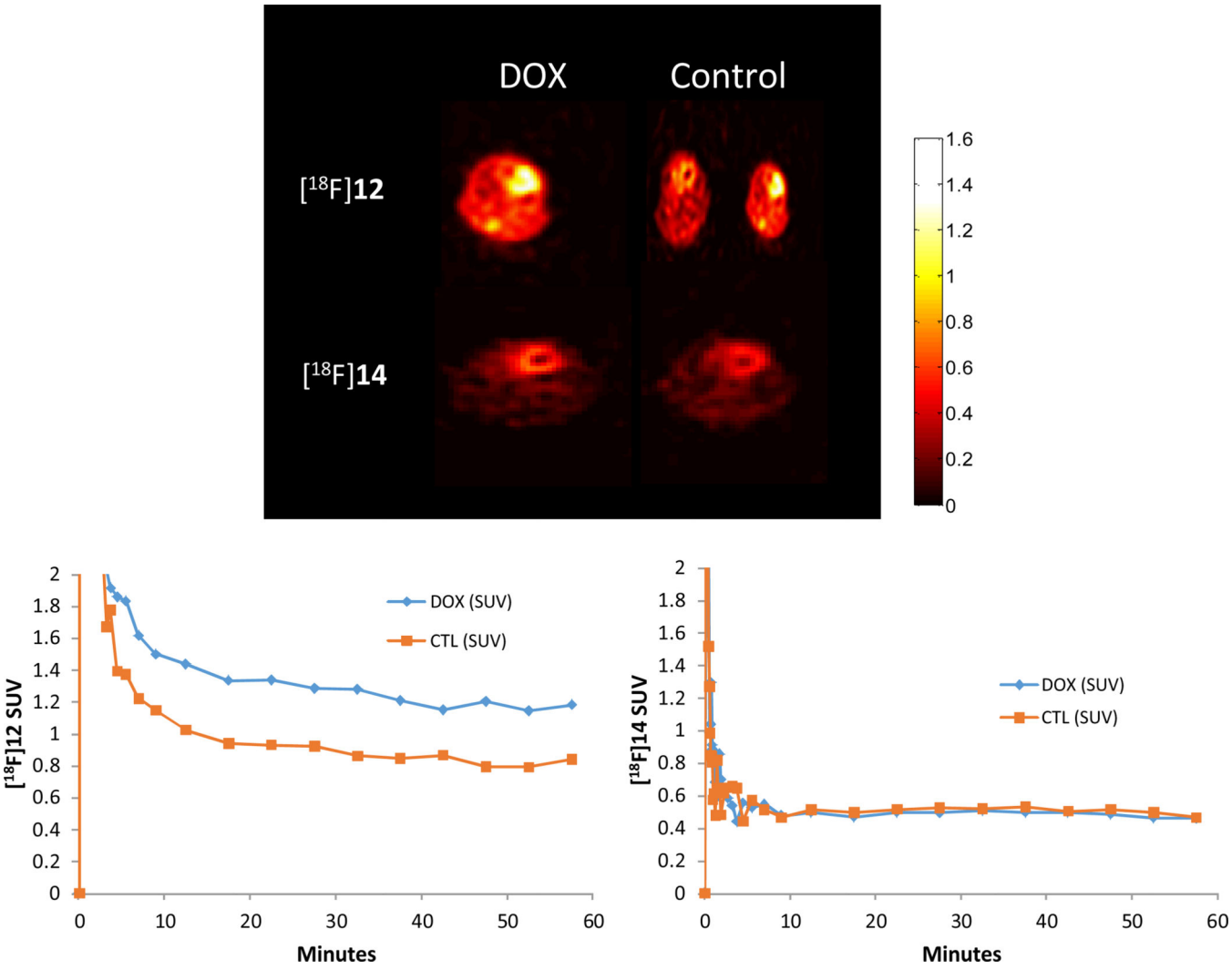


**Figure 5.**

MicroPET imaging of mice heart in untreated and DOX-treated mice with [$^{18}$F]**12** and [$^{18}$F]**14**.

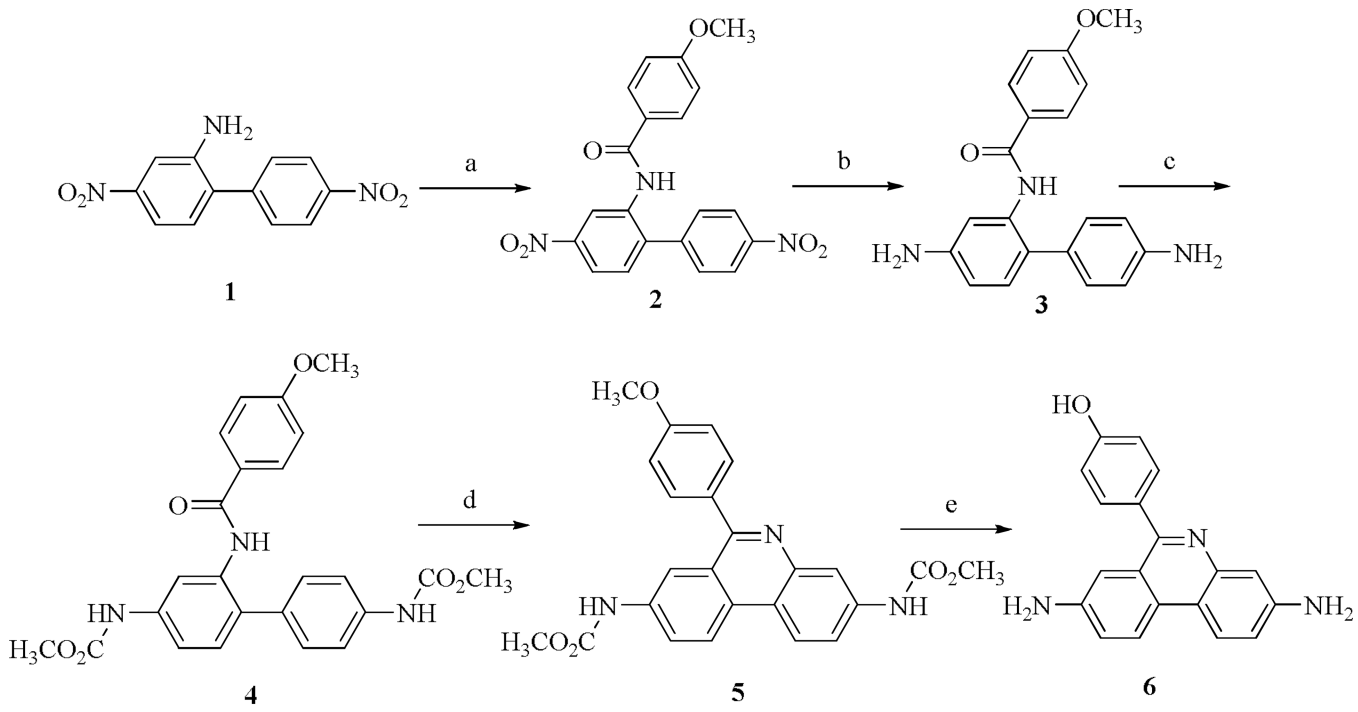


Reagents: (a) 4-methoxybenzoyl chloride, chlorobenzene, reflux; (b) $HCOONH_4$, $Pd(OH)_2/C$; (c) $ClCOOCH_3$; (d) $POCl_3$; (e) 48% HBr.

**Scheme 1.**

Synthesis of **12** and **14** (Part 1)

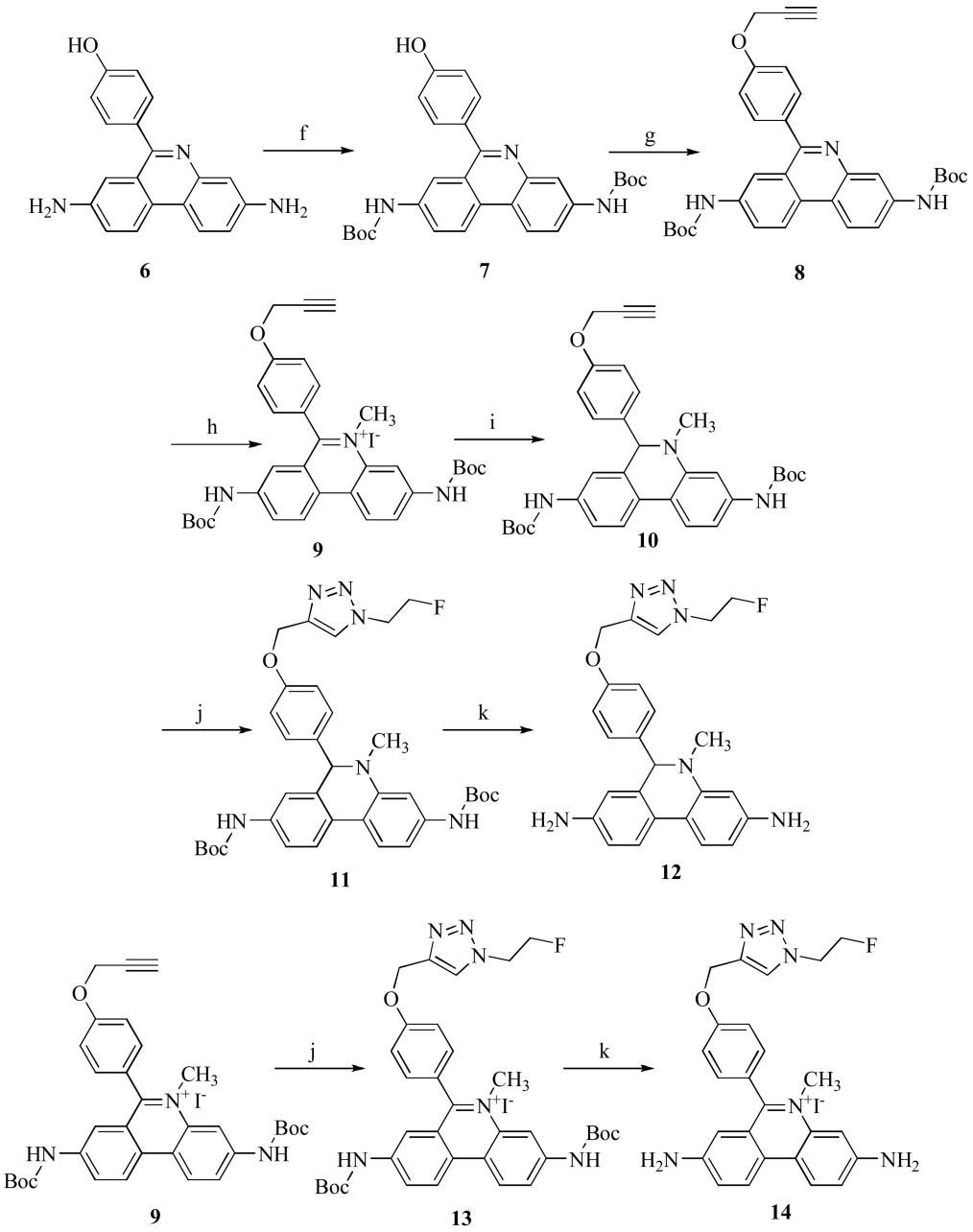


Reagents: (f) $(Boc)_2O$; (g) 3-bromoprop-1-yne, acetone, $K_2CO_3$; (h) $CH_3I$, THF; (i) $NaBH_3CN$, MeOH; (j) $N_3CH_2CH_2F$, $CuSO_4$, Sodium ascorbate, DMF; (k) EtOAc/HCl (3:1).

**Scheme 2.**

Synthesis of **12** and **14** (Part 2)

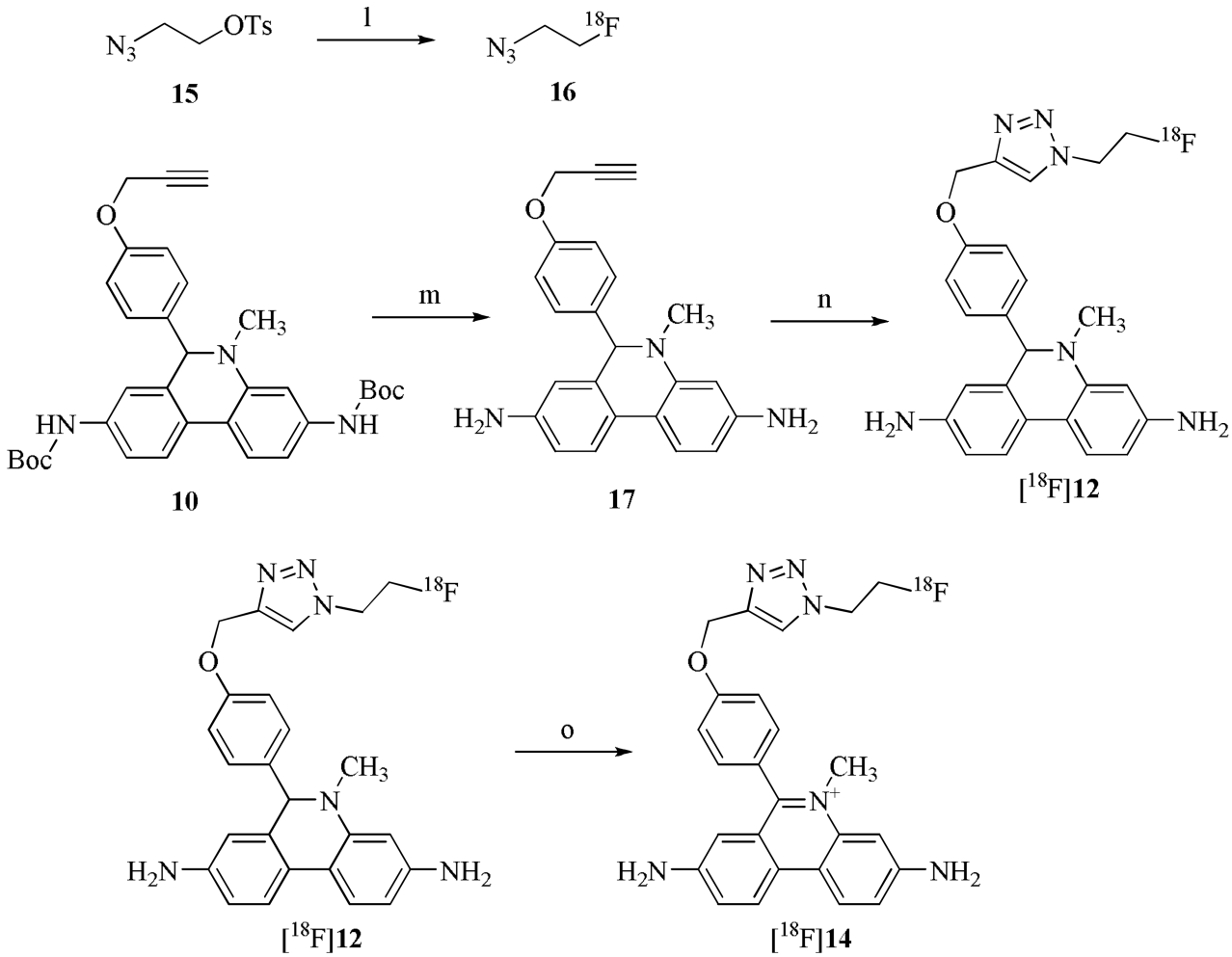


Reagents: (l) [$^{18}$F]KF, $K_{222}$, $K_2CO_3$, $CH_3CN$, 85 °C, 5 min; (m) TFA; (n) $CuSO_4$, Sodium ascorbate, DMF, DIPEA; (o) $Cu^{++}$.

**Scheme 3.**
Synthesis of [$^{18}$F]**12** and [$^{18}$F]**14**.